2 PF-Ring

2-1 Summary

The history of ring operation time, scheduled user time and actual user time since 1982 is indicated in Fig. 2. The detailed annual operation schedule for FY2007 and the operation statistics of the PF ring are summarized in Fig. 1 and Table 1, respectively. The total operation time recovered after the straight-section upgrade project in 2005, amounting to more than 5000 hours for each of the past two years, as seen in the table. In FY2007 the scheduled user time and actual user time excluding time losses due to machine trouble and daily injections were 4296 and 4177 hours, respectively. The ratio of actual user time to scheduled time has been maintained at 96-98% over the past 6 years. Figure 3 shows the trend of the product $I\tau$ of the beam current I and the beam lifetime τ over the past 11 years. The small $I\tau$ after the reconstruction work for the straight-section upgrade project gradually recovered, as seen in the figure, however, the value dropped in the spring of 2006 and in the spring of 2007. The drop in FY2006 was caused by trouble with the SR absorbers, as described in detail in the last issue of this report. The drop in FY2007 also resulted from the same cause. Figure 4 shows the history of the average stored beam current and the injection interval since 1982. Though the injection frequency in 2004 and 2005 was twice a day, it was restored to once a day in FY2007. The failure rate history (the ratio of failure time to total operation time) is shown in Fig. 5. This rate was around 1% throughout the 1990s, but has been kept to around 0.5% over the past several years. However the rates of 0.85% in FY2006 and 1.8% in FY2007 are considerably larger, due to the absorber trouble.

In FY2007 the initial beam current of 450 mA in 2.5 GeV multi-bunch mode was unchanged, and the injection frequency was maintained at once per day. The ring was operated for one week in the 3 GeV multibunch mode, and there were two one-week periods of 2.5 GeV single-bunch operation. During 3 GeV operation, the beam current was limited to 200 mA due to RF power limitations.

Table 1 Operation statistics of PF in FY2007.

	Multi-bunch	Single-bunch	Total
Ring Operation Time (hours)	4816.0	288.0	5104.0
Scheduled user time (hours)	4008.0	288.0	4296.0
Actual user time T (hours)	3894.2	282.9	4177.1
Time used for injection (hours)	26.0	1.3	27.3
Integrated current in T (A×hours)	1368.1	13.7	1381.8
Average current in T (mA)	351.3	48.4	--
Number of injections	173	64	237
Interval between injections (hours)	22.5	4.4	--

Timetable of the Machine Operation in FY2007

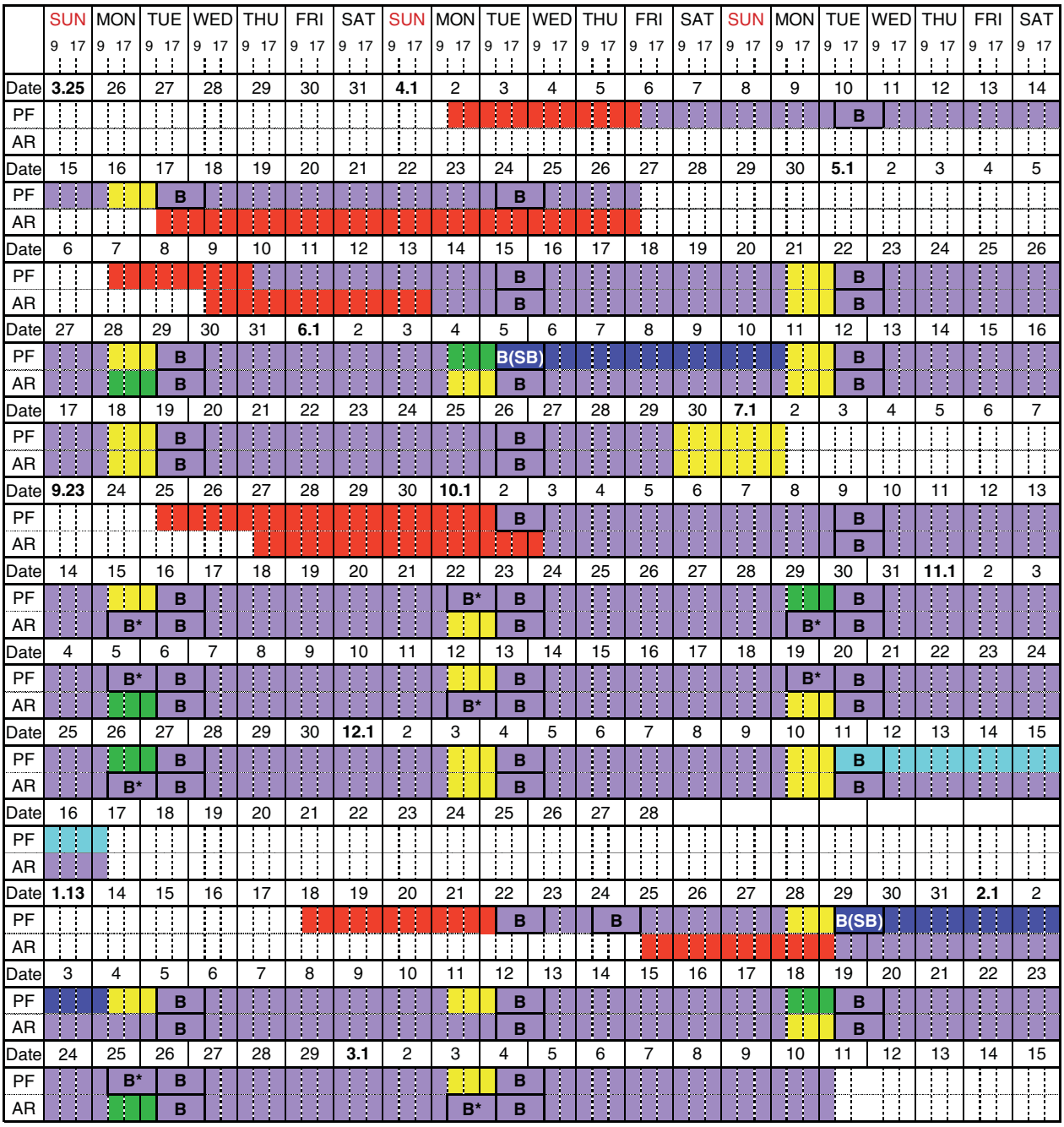

Note) 'B*' in the table is a bonus time that the ring has the priority, limited in FY2007.

Figure 1
Timetable of machine operation in FY2007.

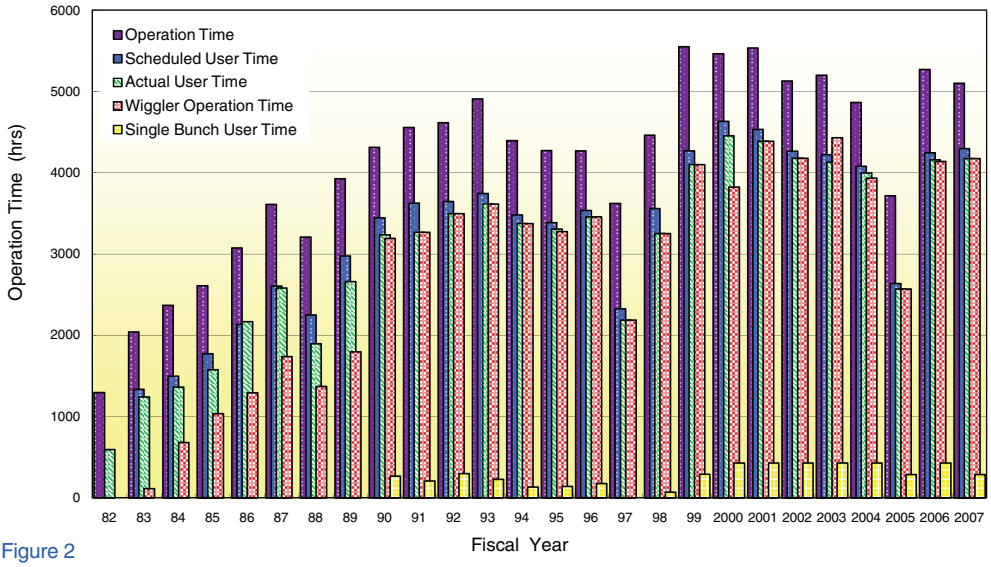

Figure 2
Operation time history of the PF Storage Ring.

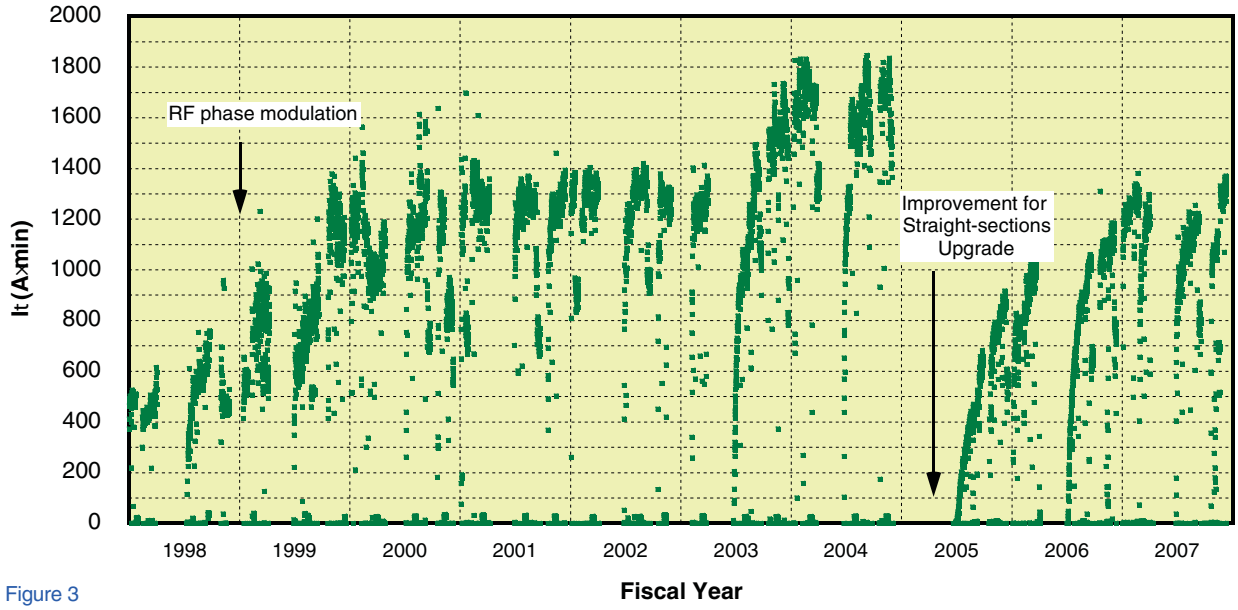

Figure 3
Iτ history of the PF Storage Ring over the past 10 years.

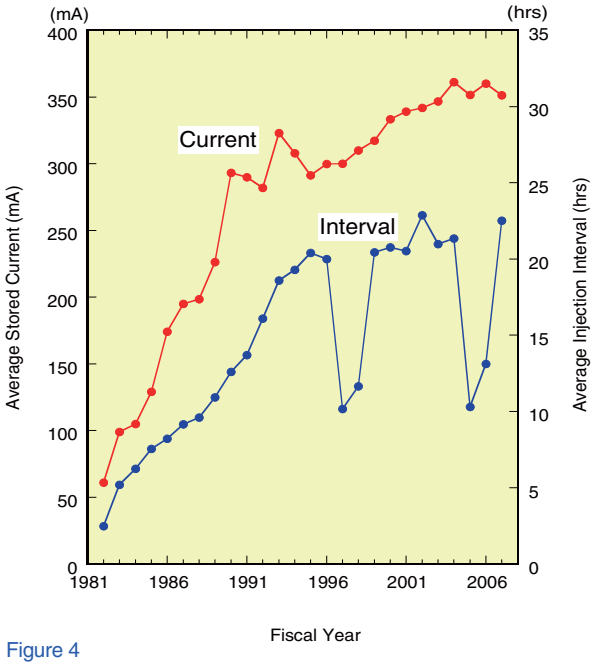

Figure 4
Average stored current and injection interval since 1982.

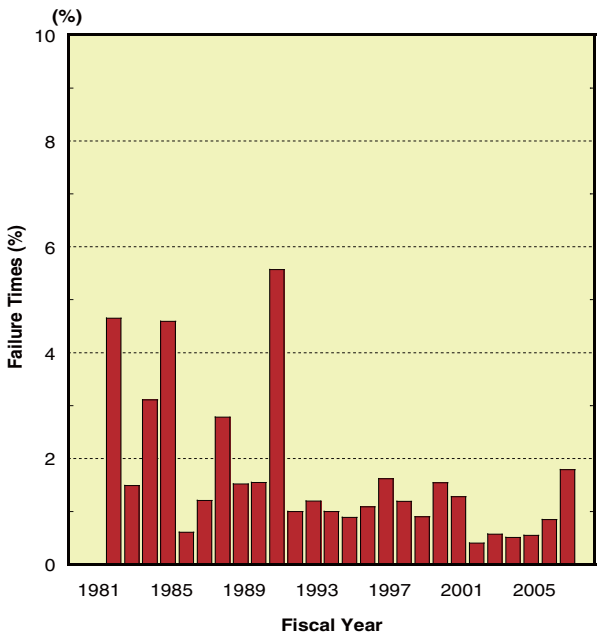

Figure 5
Failure rate history.

2-2 Development of a Polarization-Switching Source

As one of the most important subjects after the straight-sections up-grade of the Photon Factory [1], we have been developing a rapid polarization-switching source at the straight section between the bending magnets B15 and B16 in the PF 2.5 GeV ring. The source was originally planned to switch between left-handed and right-handed circular polarization at a rate as high as 10 Hz in the energy region of 200-1000 eV. Later the importance of switching linear polarization (horizontal and vertical and/or +/-45 deg.) as well as the circular polarization was recognized. We decided to construct undulators in an APPLE (Advanced Planar Polarized Light Emitter)-II type magnetic configuration [2], which can be used to produce all of these polarization states. In our plan two identical polarizing-undulators are to be installed in tandem in the B15-16 straight section. Differently polarized SR from each undulator is introduced alternately to the beamline by rapidly switching the horizontal bump-orbits of the electron beam using five kicker electromagnets [3]. The design of the undulators and the construction of one of these (U#16-1) are reported below.

U#16-1 is a polarizing undulator which has a period length of 56 mm and a periodicity of 44, designed to be a soft X-ray source covering the energy region from 200 eV to 1 keV in the 2.5 GeV PF ring. The undulator has two major operation modes, described on the basis of the symmetry of the four magnet arrays which comprises U#16-1, as shown in Fig. 6: (a) a symmetric mode and (b) an anti-symmetric mode. In the symmetric mode, two pairs of diagonal magnet arrays are simultaneously displaced longitudinally in opposite directions

(a)

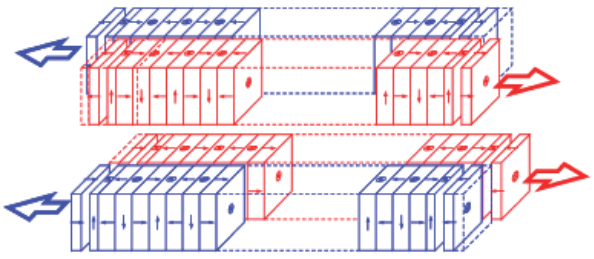

(b)

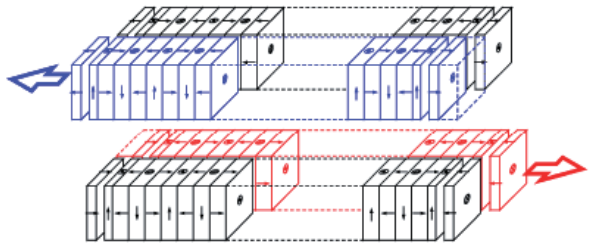

Figure 6
(a) Symmetric operation mode of U#16-1.(b) Anti-symmetric operation mode of U#16-1.

(a)

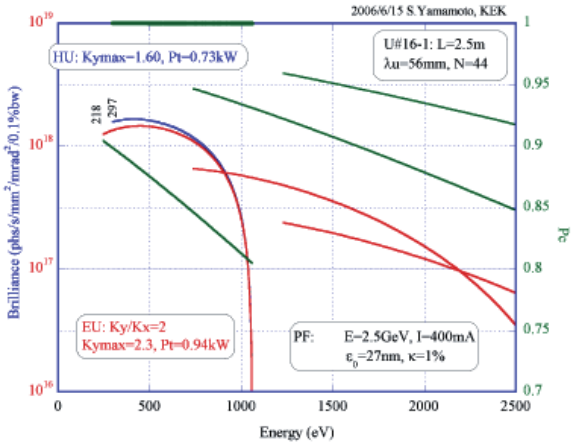

(b)

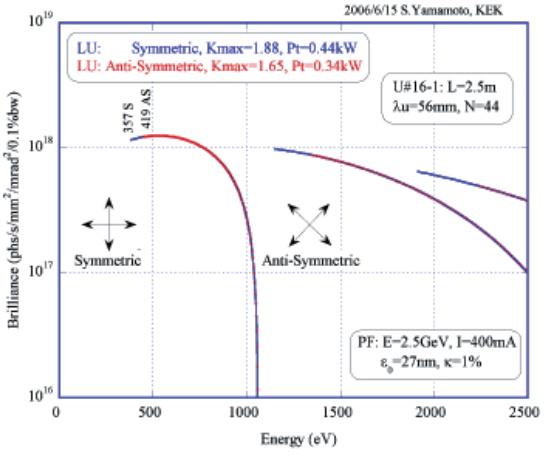

Figure 7
(a) Calculated spectra of the radiation from U#16-1 in the symmetric mode. (b) Calculated spectra of the radiation from U#16-1 in the anti-symmetric mode.

with a phase difference of δ_S. This mode can be used to obtain various polarization states of the synchrotron radiation, from horizontally linear to vertically linear through circular (elliptical). In the anti-symmetric mode, one diagonal pair is fixed at its original position, and the two arrays of the other pair are displaced longitudinally in opposite directions with a phase difference of δ_A. This mode only provides linear polarization, but the polarization plane can be rotated from horizontal to vertical. The rotation direction is chosen by the selection of one of the two possible diagonal pairs. Figure 7 shows examples of the spectra of the radiation from U#16-1 in: (a) the symmetric mode and (b) the anti-symmetric mode.

When constructing U#16-1, we employ a pure Halbach type magnet arrangement for each of the four magnet arrays. For the magnet material we have selected Nd-Fe-B alloy with a remanent field B_r=12.5 kG and a coercivity iH_c=25.0 kOe (NEOMAX38VH manufactured by NEOMAX Co. Ltd.), because of its excellent magnetic performance. The magnet blocks are coated with TiN (5-μm thick). The magnet gap ranges from 220 mm to 21 mm (with the deflection parameters K_x and K_y ranging up to 1.6 and 2.3, respectively).

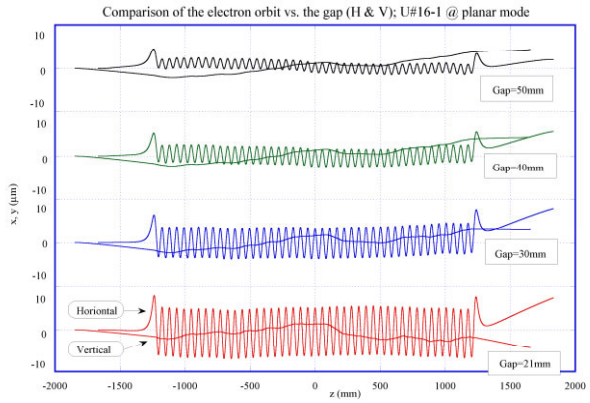

Figure 8
Summary of the field adjustments of U#16-1 (λ_u=56mm). Electron orbits in the x- (horizontal) and y- (vertical) directions are shown at several gaps.

Field adjustments have been made on the basis of precise field measurements at a gap of 21 mm in the symmetric mode with δ_S=0. For this purpose, we devised a new magnetic detector using Hall probes which are oriented in the y- and x- directions. The sensor part of the detector is formed to fit in a gap as small as 10 mm, and is a kind of a micro-oven of Cu equipped with a thermistor-type thermometer and heaters. The temperature of the detector is controlled to an accuracy of 0.01°C. We have adjusted the undulator field by optimizing the kick angle of the electron beam at each pole in order to have an ideal sinusoidal orbit in the horizontal plane and also a straight orbit in the vertical plane. For the adjustment method we employ: (1) exchange of the magnet blocks and (2) insertion of shims to retract the magnet blocks outward in the horizontal plane.

The electron orbits in the undulator are summarized in Fig. 8. The quality of the undulator fields is kept satisfactory over the whole gap range. We also have satisfactory results on the kicks at the undulator's entrance and exit, where parallelism between the electron orbit and the undulator is violated. We find that the absolute values of the kicks and their relative changes are satisfactorily small. The field errors are evaluated in terms of optical phase errors. The root-mean-square error of the optical phase is as small as 2.0 degrees.

When we use U#16-1, we can select the desired magnetic field (horizontal or vertical) and polarization states by changing the magnet gap and δ_S or δ_A. In the symmetric mode, the values of δ_S are well explored to realize cases of $K_x = K_y$ (circular polarization) or $K_x = K_y/2$, which are of importance for the actual use of U#16-1. In the anti-symmetric mode, δ_A values to realize +/-45 deg. polarization states have been determined. Besides these basic methods, if an additional phase φ is introduced between the upper two magnet arrays and the lower two arrays with a constant gap and δ_S in the symmetric mode, we can obtain the desired magnetic field strengths for a constant polarization state without changing the magnet gap, as shown in Fig. 9a[4]. Also in the anti-symmetric mode, if we set φ between the upper and lower arrays at constant gap and δ_A, we can rotate the polarization plane with constant field strength (*i.e.* constant radiation energy), as shown in Fig. 9b. Here, we have to set $\delta_A = \delta_C$, where the value of δ_C corresponds to circular polarization in the symmetric mode.

For a gap of 21 mm, the magnetic field strength with circular polarization is well controlled by the additional phase φ, as exemplified in Fig. 10. The above methods are additional, but important to simplify the operation of U#16-1.

After the field adjustments described above, U#16-1 was installed into the PF ring together with its vacuum chamber. The chamber was made of stainless steel, and the inside surface electrolytically polished. The inner diameter of the chamber is designed to be 15 mm (19 mm outer diameter) to allow for a minimum magnet gap of 21 mm. The vacuum chamber is evacuated with a combination of non-evaporable getter (NEG) pumps and sputter ion pumps (SIP). Since the total length of the B15-16 straight section is 8.9 m, and the vertical aperture of this section is only 15 mm, some problems due to resistive wall instabilities can be anticipated for chambers made of resistive materials such as stainless

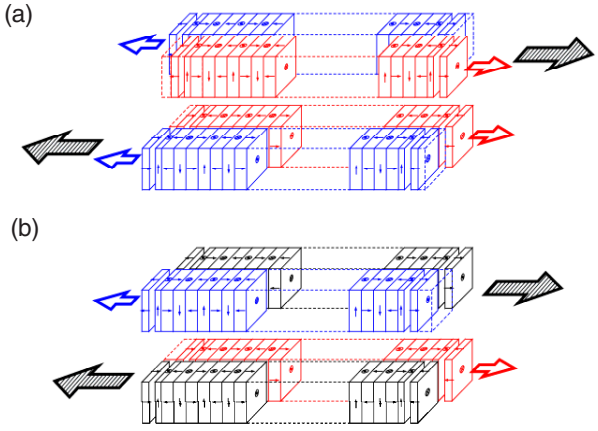

Figure 9
(a) Additional phase ϕ in the symmetric mode of U#16-1.
(b) Additional phase ϕ in the anti-symmetric mode of U#16-1.

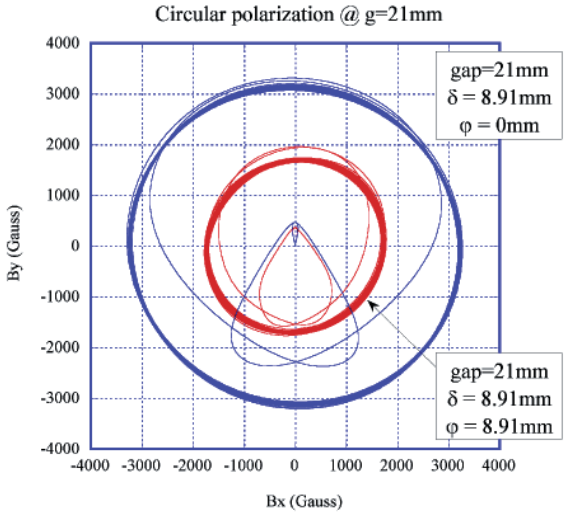

Figure 10
Magnetic field strength is controlled by an additional phase ϕ at a constant gap of U#16-1.

steel [5]. In order to prevent this, we have plated the inside walls of the chamber with Cu to a thickness of 100 μm over the region of the electron beam path.

Various machine studies are now underway, including the commissioning of U#16-1 and the development of bumped orbits for rapid polarization switching.

REFERENCES

[1] T. Honda, S. Asaoka, W.X. Cheng, K. Haga, K. Harada, Y. Hori, M. Izawa, T. Kasuga, Y. Kobayashi, H. Maezawa, A. Mishina, T. Mitsuhashi, T. Miyajima, H. Miyauchi, S. Nagahashi, T. Nogami, T. Obina, C.O. Pak, S. Sakanaka, H. Sasaki, Y. Sato, T. Shioya, M. Tadano, T. Takahashi, Y. Tanimoto, K. Tsuchiya, T. Uchiyama, A. Ueda, K. Umemori and S. Yamamoto, *AIP Conf. Proc.,* **879** (2007) 87.
[2] S. Sasaki, *Nucl. Instr. And Meth.,* **A 347** (1994) 83.
[3] *Photon Factory Activity Report 2007*, **25A** (2008) 107.
[4] T. Schmidt and D. Zimoch, *AIP Conf. Proc.,* **879** (2007) 404.
[5] N.Nakamura, private communication.

2-3 A Fast Local Bump System for Helicity Switching at BL-16

In order to detect the weak signals which arise when using the lock-in technique to study the photon polarization dependence of materials, fast helicity switching system of the undulator radiation is required. To this end a fast local orbit bump system has been developed at BL-16, in the south straight section of the PF ring. The conceptual design of the system is shown in Fig. 11. The bump system consists of five identical fast bending magnets and power supplies, which were manufactured in 2007. After magnetic field measurements and frequency response measurements, the system was installed during the spring shutdown in 2008. In this section, we present the parameters of the system, along with the results of the magnetic field and frequency response measurements.

Table 2 Principal parameters of the system.

Max. beam energy	E [GeV]	3
Max. kick angle	θ [mrad]	2.4
Max. magnetic field (3GeV)	B [T]	0.16
Vertical pole gap	h [mm]	21
Horizontal pole width	w [mm]	110
Magnet core length	l [mm]	150
Coil turn number	N [turns]	32
Inductance	L [H]	1.0×10^{-3}
Maximum magnetic current (3GeV)	I [A]	83.5
Resistance	R [Ω]	0.1
Design bump frequency	f [Hz]	10
Max. voltage for 10Hz operation	V [V]	13.7
Silicon steel thickness	t [mm]	0.5
Power supply capacity	I [A]	±100
	V [V]	±50

For the lock-in technique at the user beam line, the required switching frequency is more than 10 Hz. In order to separate the photons from the two undulators of different helicities, an angle bump of 0.3 mrad is necessary in the undulators. Thus the maximum required kick angle is 2.4 mrad from the geometrical configuration. For a beam energy of 3 GeV, the required magnetic field is about 0.16 T. The parameters of the magnets and power supplies are given in Table 2.

Before the installation of the system in the ring, magnetic field and frequency response measurements were conducted. Figure 12 shows the excitation curve measured using a Hall probe (F.W.BELL 9500A). The magnetic field is about 0.19 T at a current of 100 A. We also measured the horizontal (Fig. 13)

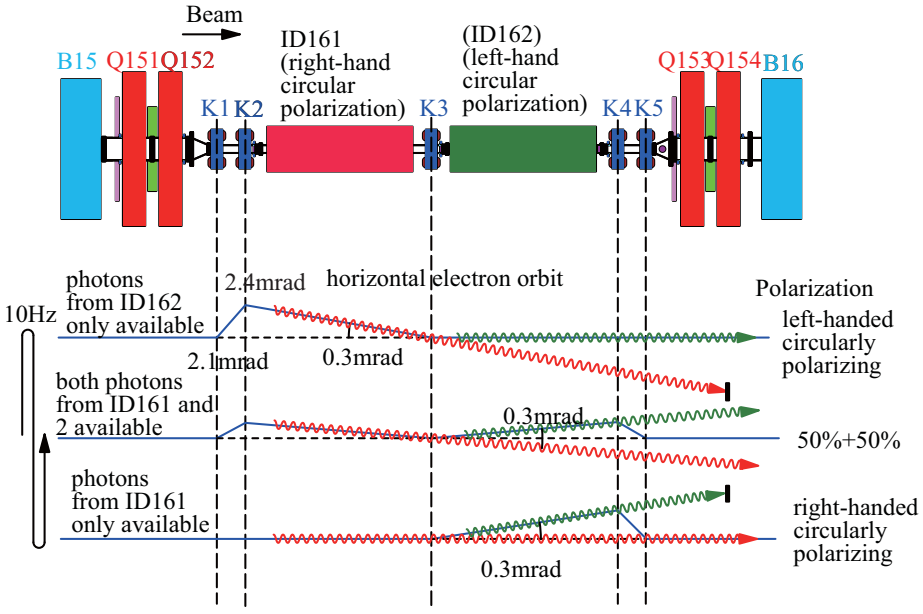

Figure 11
Schematic drawing of the conceptual design for producing fast helicity switching.

and longitudinal (Figure 14) magnetic field distributions. Over the region |x| < 35 mm the magnetic field distributions are so flat that $\Delta B/B$ is smaller than 1×10^{-3}, which is adequate for beam injection. Since the length of the magnetic core is 150 mm, the effective length is 183 mm. Figure 15 shows the delay of the phase measured using a FFT analyzer (HP 3562A). For a switching frequency of 10 Hz the delay of the phase of the sinusoidal magnetic field from the power supply control signal is about 0.7 degrees with no vacuum duct, and 5.8 degrees with a vacuum duct made from 2 mm thick SUS. The attenuation of the magnetic field by the vacuum duct is less than 0.1%, almost negligible. Differences in frequency responses between the five magnets and power supplies were very small and independent of magnetic current.

During the spring shutdown of 2008, the bump system was installed into the PF ring. For aligning the magnets a levelling scope (Wild N3), a theodolite (Kern T3000), a metal ruler and a water level were employed. The tolerances of the maximum errors were 0.1 mm for the transverse position, 0.5 mm for the longitudinal position, and 0.2 mrad for the rotation error of the magnetic poles. After the alignment, the maximum alignment error was reduced to 0.06 mm for the horizontal and vertical positions, 0.5 mm for the longitudinal position, and 0.04 mrad for the rotation. Figure 16 shows the bump system with one undulator installed in the PF ring.

Machine studies with beams were begun in May, 2008.

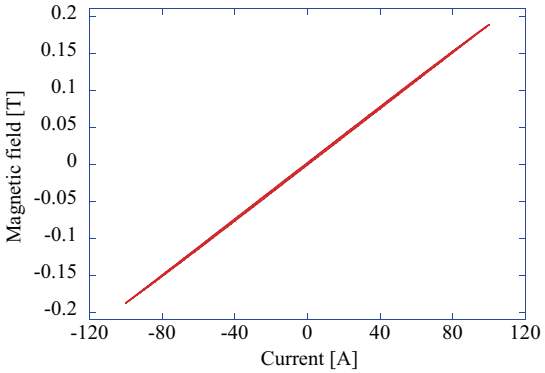

Figure 12
Typical excitation curve of the magnet.

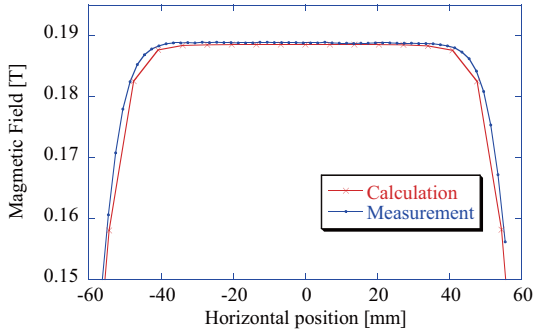

Figure 13
Typical horizontal distribution of the magnetic field at a magnetic current of 100 A. The solid blue line and red crosses show the results of the measurement and the calculation, respectively.

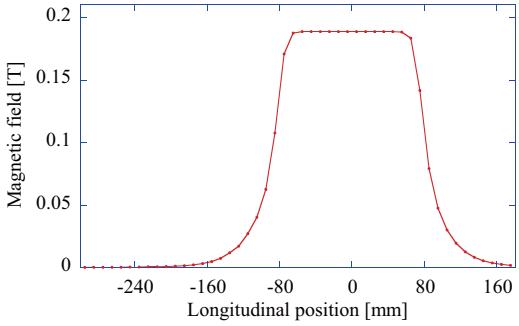

Figure 14
Typical longitudinal field distribution of the magnetic field at a magnetic current of 100 A.

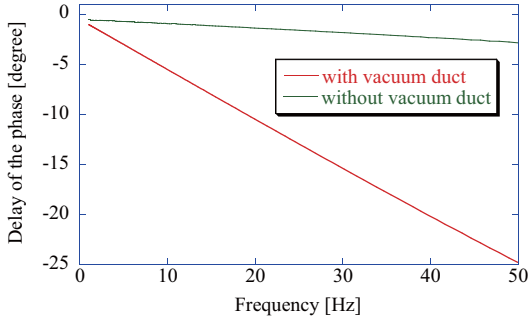

Figure 15
Typical phase delay as a function of frequency with a magnetic current of 50 A. The two lines represent the phase delay with (red) and without (green) a vacuum duct.

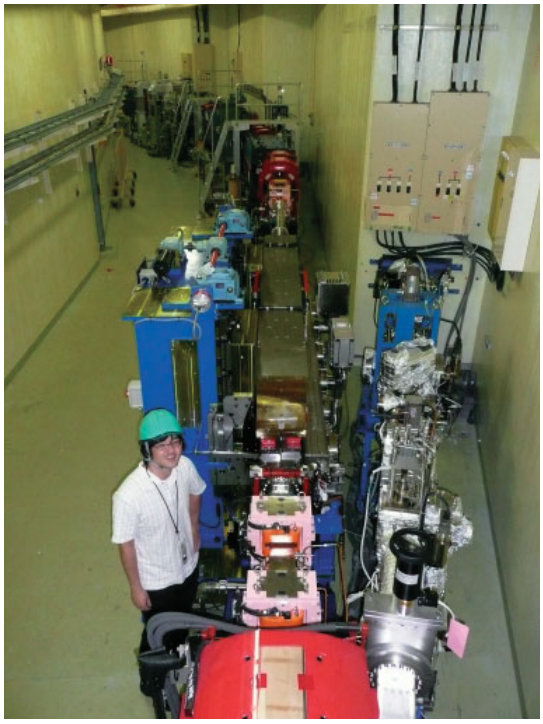

Figure 16
The south straight section of the PF-ring. In the centre of photograph is the APPLE-II type undulator U#16-1. The pink magnets are the bump magnets for switching.

2-4 PF Top-Up Injection

1. Injector Upgrade for PF Top-up

The KEK injector linac provides the beams of different modes sequentially with four storage rings: Low Energy Ring (LER) of KEKB (3.5 GeV/ e^+), High Energy Ring (HER) of KEKB (8 GeV/ e^-), Photon Factory (PF; 2.5 GeV/ e^-) and Advanced Ring for Pulse X-rays (PF-AR; 3 GeV/ e^-). The PF and PF-AR rings take a beam injection twice daily, whereas the KEKB rings are operated under continuous injection mode (CIM) in order to keep the stored current almost constant. The KEK Linac upgrade project has been in progress since 2004 so that the PF Top-up and KEKB CIM can be performed at the same time. The final purpose of this upgrade is to change the linac parameters (beam mode) up to 50 Hz of the maximum linac beam repetition by using a multi-energy linac scheme. In this scheme, the common magnet settings for the KEKB and PF rings are used. The beam energy is adjusted rapidly by quick control of low-level RF phase.

In the winter of FY2007, a pulsed bend was installed upstream of the PF-BT instead of the previous DC switch bend (Fig. 17). The pulsed bend can create 7-deg. bends in a beam of up to 3 GeV, and its maximum repetition is 25 Hz. The current shape applied to the magnet is a half-sinusoidal pulse of 32-kA amplitude and 200-μs pulse length. We have also installed a 1200-mm-long ceramic chamber coated with 1-μm-thick Ti. The pulsed bend has been used for daily operation without any trouble since January 2008.

For the fast beam-mode switch between KEKB electron and positron modes, the positron production target with a hole will be used. We will control quickly the primary electron beam position and angle at the positron target. The positron target is crystalline tungsten with 5-mm diameter. The center of a hole is placed 4.5 mm apart from that of the tungsten target, and the hole diameter is about 3 mm. The e^- beam passes within the hole for the e^- mode, but hits the center of the tungsten target for the e^+ mode. For fast control of the primary electron beam orbit, four pulsed steering magnets were installed in the winter of FY2007. The preliminary test was successful, and the development of operation software is ongoing.

For the KEK Linac upgrade, it is also indispensable to upgrade the timing system. In the current timing system, about 150 timing delay modules based on VME-bus (TD4V) and CAMAC (TD4) are used for controlling the timing signals distributed to the many different types of local controllers. The event generator and receiver (EVG/EVR) system based on VME64x-bus will be adopted as the new timing system as shown in Fig. 18. In the new system, EVG and EVR are connected by optical fiber. The event information (beam mode), RF clock (114 MHz), timestamp and data buffer can be quickly transferred from EVG to EVR. In addition, the number of modules used for the timing system can be drastically reduced by using the EVG/EVR system. This dramatically increases the reliability of the timing system and beam operation. The development of operation software based on the EPICS system has almost been completed. The preliminary machine study was carried out by using only one EVG/EVR combination. In this study, we attained fast control of two different beam energies in every pulse of 50 Hz, and satisfactory results were confirmed with a fluorescent screen monitor as shown in Fig. 19. The overall system test will be carried out towards practical operation.

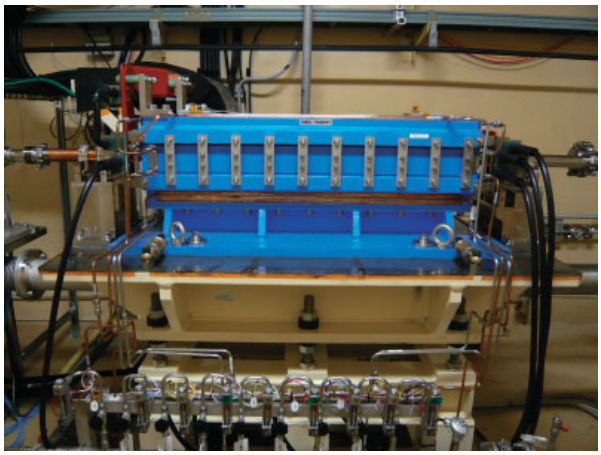

Figure 17
Photograph of pulsed bend.

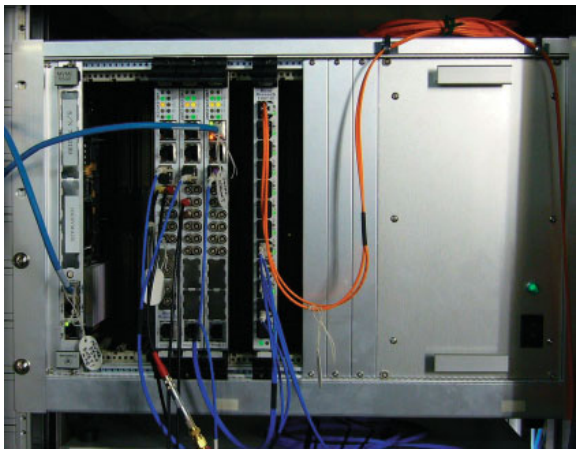

Figure 18
Photograph of new timing system (event generator/ reciever).

Figure 19
Machine study result for fast beam energy switch with a new timing system.

2. Status of the PF ring

During FY2007, two slits were installed in the beam transport line to eliminate beam halo and energy tail of the linac beam. A beam dump line was constructed for the beam regulation of linac during top-up operation using beam transport line. During June 2007, the PF ring was injected keeping the beam shutter open in multi-bunch user operation, a top-up operation was routinely performed during single-bunch user operation in January 2008. A longitudinal feedback system was also successfully tested in 2007.

3. Installation of slits in the beam transport line

Because the beam from linac has certain beam halo and energy tail. These beam halo and energy tail will increase beam loss during injection. Consequently, radiation level of the SR beamline will sometimes increase when the beam shutter is opened during the injection. To keep radiation level of SR beamline lower than allowed level of experimental hall, we must eliminate beam halo and energy tail from the linac beam. For this purpose, two slits are newly added in the beam transport line. First slit is set at the large dispersion section to limit energy spread of linac beam within the acceptance of energy aperture of the ring. The second slit is set near the end of beam transport line to eliminate the beam halo. Using these slits, radiation level of SR beamlines became sufficient lower than allowed radiation level of the experimental hall. Photographs of these two slits are shown in Fig. 20 and Fig. 21.

4. Construction of the beam dump line

In the conventional operation, the beam regulation for the injection is done by Linac mode with the conditions of beam transport magnets OFF, and keeping MBS closed. In this mode, beam will not come to the beam transport line. Since under the top-up mode, all magnets in the beam transport line are ON, the beam from linac always can come to the end of beam transport line. When some trouble will happen in the Linac during continuous injection in the top-up mode, we must do some beam regulation under keeping top-up mode operation. We must prevent the increase of radiation level of SR beamline due to the poor quality beam during the linac regulation. For this purpose, a beam dump line was newly constructed and added near end of beam transport line. Photograph of the beam dump line is shown in Fig. 22. This dump line is also use to research and development of beam instrumentation.

5. Operation of top-up injection mode during single bunch user operation

We operate a single bunch user operations in June 2007 with keeping the MBS opened during injection. Typical one-day history of the ring current in this run is shown in Fig. 23. Due to short lifetime in the single bunch operation, the beam is injected 8 times a day with almost constant interval.

In the single bunch user operation in January 2008, the PF ring was operated with top-up mode. The ring current duration was recovered with 3 second injection in every 10 secnd with injection rate of 0.01 mA/sec. The top-up injection is interrupted twice daily by PF-AR injections. Typical one-day history during this run is shown in Fig. 24. In this figure, we can see two drops in current due to injection of the PF-AR ring. The detail of injection pattern is shown in Fig. 25. The injection rate is controlled by slit which set at near end of beam transport line as mentioned in previous section. Accidental interruptions in this operation are listed in Table 3. Re-

Figure20
First slit in the large dispersion section to limit energy spread.

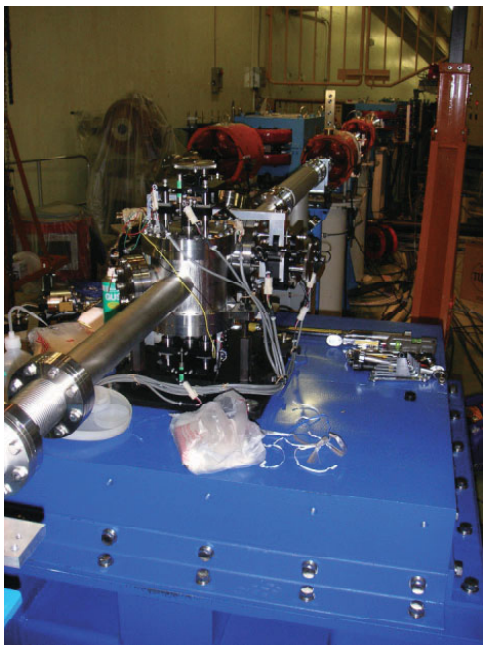

Figure 21
The second slit is set near the end of beam transport line to eliminate the beam halo.

Table 3 Accidental interruptions in one week single-bunch Top-up operation

Source of interruptions	Number of interruptions	Recovery time
Irregular injection for the PFAR	once	14min
Linac Klystron fault	2 time	8min
Linac sub-booster klystron fault	once	5min
Linac beam energy regulation	3 times	7min
Timing system fault	once	27min

covery time for the interruptions are also listed in this table. Linac klystron faults are normally recovered from in less than several ten seconds, but more than a few min were taken in this run. An interruption due to injection timing system occurred and it takes 27 min for recover.

6. Schedule

The fast switching system will be installed until the end of 2008. Following this installation, it will be possible to test the fast switching mode of the multi-energy Linac scheme. This testing is scheduled in spring operation in 2009. After these testing, the top-up user operation during the B-factory electron injection mode will plan to start on autumn operation in 2009. Otherwise, we plan to operate all the single bunch operations in 2008 with top-up operation.

The PF ring can operate with top-up mode during the B-factory electron injection mode, since the electron beam is not available when the B-factory is being injected with positrons. We installed a special target which has a hole in the side to allow electron beam acceleration even during the positron operation. The electron beam is pass hole in the side of target by pulse bump orbit. This target is often tested during user operation of the PF.

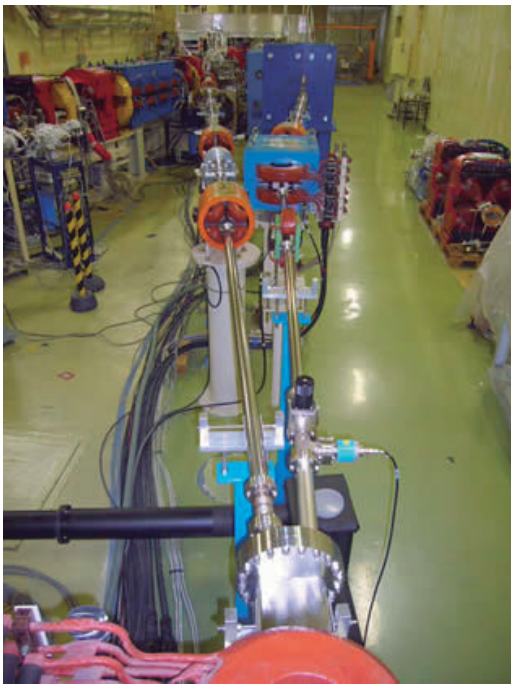

Figure 22
Beam dump line added near end of beam transport line. The left line is injection line, and right line is new beam dump line.

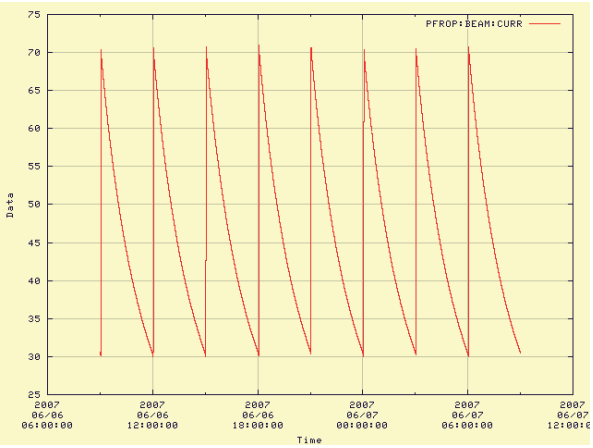

Figure 23
Typical one-day history of the ring current. The beam is injected 8 times a day with keeping MBS opened.

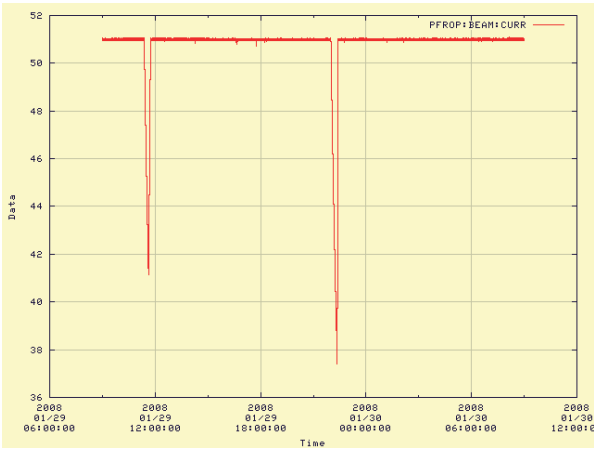

Figure 24
Typical one-day history in the single bunch user operation in January 2008 with top-up operation.

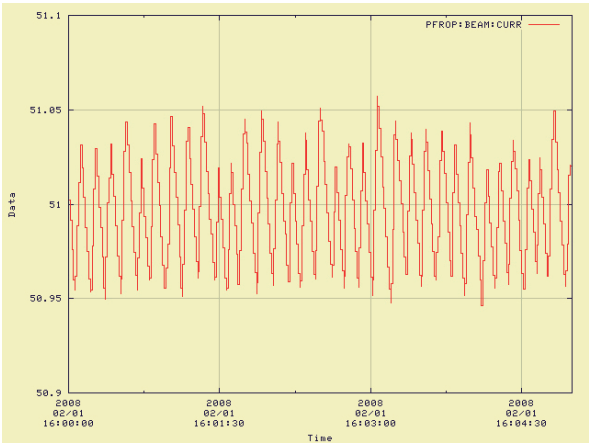

Figure 25
The detail of injection pattern in the top-up operation. The ring current is recovered with 3 seconds injection in every 10 seconds with injection rate of 0.01 mA/sec.

2-5 Development of a Longitudinal Bunch-by-Bunch Feedback System

In multibunch operation, several longitudinal coupled-bunch mode instabilities are observed for stored ring currents above 50 mA, and many efforts have been made to suppress these instabilities [1-3]. After the successful completion of the mode feedback system together with a preliminary digital signal processing system [2-3], a full bunch-by-bunch feedback system has been developed. A general purpose signal processor, the iGp, has been developed by a collaboration between KEK, SLAC, and INFN-LNF [4-5]. The iGp provides real-time baseband signal processing at an RF frequency of 500 MHz for the 312 bunches at the PF. The longitudinal position of each bunch is digitized by an 8-bit ADC, processed by a 16-tap finite impulse response (FIR) filter, and transmitted to a DAC after the introduction of an appropriate delay. A digital filter is implemented using a field-programmable gate array (FPGA). A block diagram of the bunch-by-bunch feedback system is shown in Fig. 26.

Figure 27 shows typical beam spectra recorded with and without the feedback system. In order to observe differences from the present SR user's operation, we tested the four patterns of operation listed below. Hereafter 'PM' indicates RF phase modulation, and 'FB' indicates the bunch-by-bunch feedback system.

(A) FB OFF, PM ON : same as present user's operation

(B) FB ON, PM ON : both systems ON

(C) FB ON, PM OFF: only feedback system; ideal case.

(D) FB OFF, PM OFF: no beam stabilization

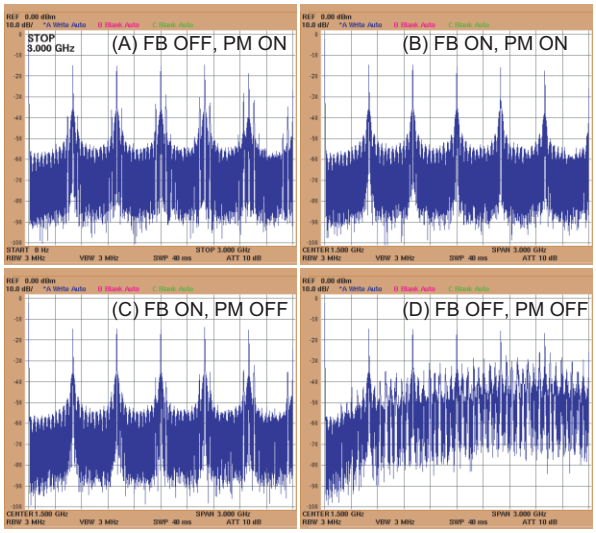

Figure 27
Beam spectra measured using a button-type pickup electrode. The frequency span is from 0 to 3 GHz. FB indicates feedback and PM indicates phase modulation of the acceleration RF signal.

The beam current during these measurements was selected to be 430 mA, and 280 bunches were stored in the 312 available buckets to prevent the onset of transverse ion-trapping instabilities. The beam spectra recorded using a button-type pickup electrode with feedback conditions (A)-(D) are shown in Figs. 27 (A)-(D), respectively. The frequency range is from DC to 3 GHz. In Fig. 27(A), harmonics of the RF frequency are observed at 500 MHz, 1 GHz, 1.5 GHz, … Spectral lines corresponding to the longitudinal coupled-bunch mode instabilities of mode number 276 (or mode –36) are also observed. In some cases, mode 276 disappears and another mode, mode 195 (–117), is observed (not shown in the figure). With both PM and FB turned ON (Fig. 27(B)), all of the instability lines disappeared and only the RF harmonics were observed. Beam stabilization appears to be successful, although the energy

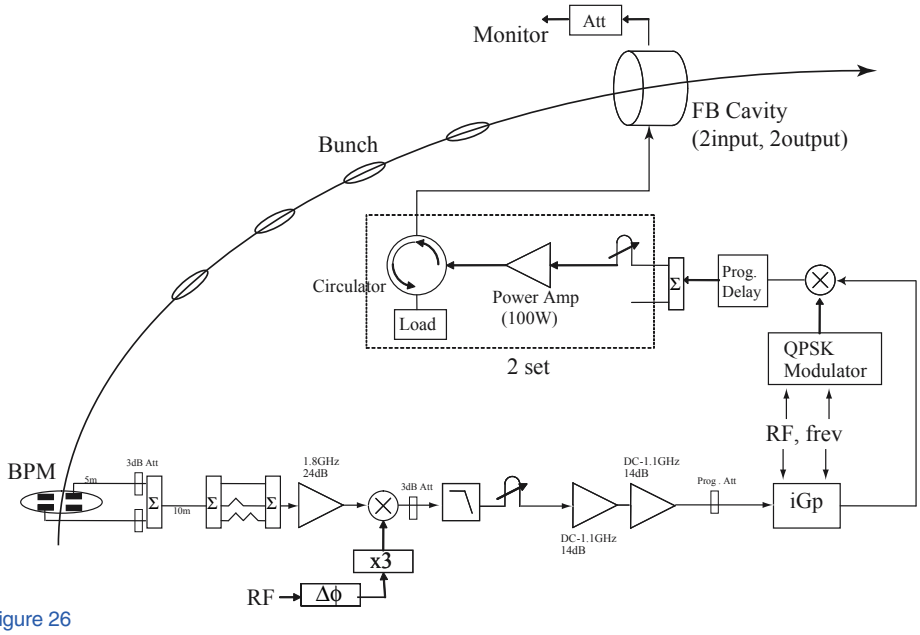

Figure 26
Block diagram of the bunch-by-bunch feedback system.

spread of the bunch is still large, a condition which is not advantageous for SR experiments. With no stabilization at all (Fig. 27(D)), several instability modes are observed. The strength of each mode is not constant, and the peak heights vary. Figure 27(C) shows the beam spectrum without PM but with FB. This operation pattern is the ideal case for feedback system development. In the low-frequency region below 1 GHz there is no instability peak. On the other hand, a small peak corresponding to mode 276 exists in the high-frequency region above 2 GHz. Expanding the frequency range around the modes reveals that this peak is located 2 fs away from the revolution harmonics, and there are no peaks around fs. The dipole motion has been successfully suppressed by the feedback system and only the quadrupole-mode oscillations remain. A streak camera was used to directly observe the bunch shape, as shown in Fig. 28. The top figure shows the longitudinal bunch shape with neither FB nor PM (case (D)), and the bottom figure shows case (C). It is apparent that the feedback system suppresses dipole motion, and the bunch length varies along the bunch train. It should be noted that the adjacent bunches in Fig. 28 are actually 8 ns apart since the frequency of the fast-sweep signal of the streak camera is a quarter of the RF frequency. The bunch length is not constant. As time advances, the longer bunches become shorter, and vice versa. When a bunch arrives in the shortest time interval, the bunch length is shorter than the natural bunch length.

The effects of the longitudinal feedback on SR users were examined. Beamline users measured the intensity and stability of the SR while the machine was operated for approximately 2 h using each of patterns (A) to (D). The initial beam current was selected to be 430 mA. The beam current and lifetime are plotted in Fig. 29. The difference in lifetime between cases (C) and (D) indicates that the average bunch volume is increased by the quadrupole mode oscillation of the bunch. This is consistent with the beam spectra and streak camera measurements.

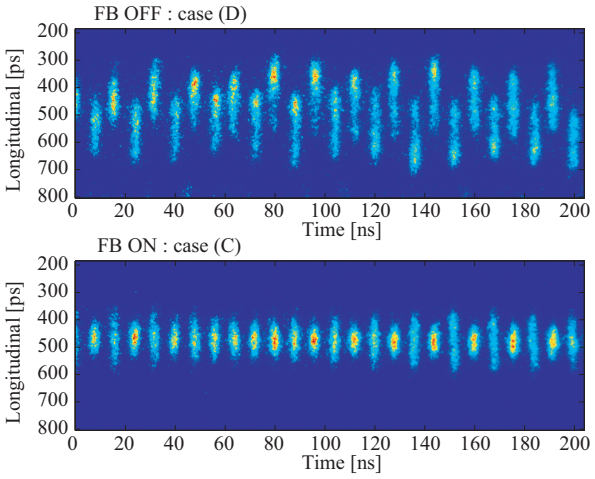

Figure 28
Longitudinal bunch shape measured using a streak camera. The top figure shows the profile without feedback (case(D)), and the bottom figure shows the profile for feedback case (C).

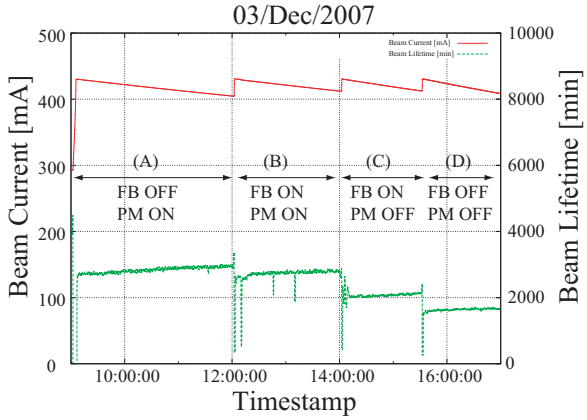

Figure 29
Beam current and lifetime while the effects of FB and PM are examined.

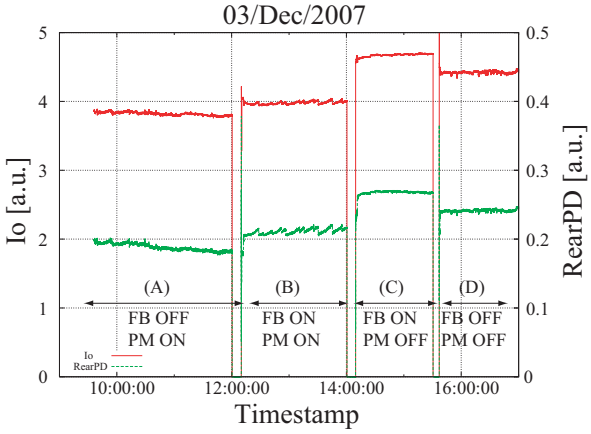

Figure 30
Intensity of SR measured at BL17. Io indicates the intensity of the input light measured using an ion chamber, and RearPD indicates the output voltage of a photo detector placed downstream of the X-ray diffractometer. Both scales are plotted with arbitrary units.

Figure 30 shows the SR intensity recorded at BL-17, a short-period small-gap undulator (SGU) in an in-vacuum configuration. Due to limitations of the lattice and available space, this undulator is installed at a non-zero dispersion region. For cases (A) and (B), fluctuations and drifts in intensity are observed. On the other hand, when the feedback loop is closed, the intensity increases by approximately 30% in case (C), with almost negligible fluctuation and drift.

At BL-5, an increase in intensity of approximately 50% was observed with feedback, with a decrease in fluctuations from 5% to 3%. At other beamlines, the effects of longitudinal feedback were not significant, and the beam quality was not degraded by the feedback. The feedback system has thus been confirmed to be very effective.

Regular multibunch SR operation starts with a stored current of 450 mA. In order to improve the highest beam current for dipole-mode suppression, two 500-W power amplifiers are ready to be installed in place of the present 100-W amplifiers.

It is also important to suppress the quadrupole-mode instabilities to maximize the intensity at the insertion device beamlines with non-zero dispersion. We are

planning to develop another feedback system for the quadrupole-mode.

REFERENCES

[1] S. Sakanaka, M. Izawa, T. Mitsuhashi and T. Takahashi, *Phys. Rev. ST Accel. Beams,* **3** (2000) 050701.
[2] *Photon Factory Activity Report 2006,* **24A** (2006) 106.
[3] W. X. Cheng, T. Obina, T. Honda, M.Izawa, M.Tadano, M. Tobiyama, T. Nakamura and K. Kobayashi, *EPAC2006* (2006) 3009
[4] D. Teytelman, C. Rivetta, D. Van Winkle, R. Akre, J. Fox, A. Krasnykh, A. Drago, J. Flanagan, T. Naito and M. Tobiyama, *EPAC2006* (2006) 3038
[5] to be published in Proc. Beam Instrumentation Workshop 2008.

2-6 Beam Injection System by Use of a Pulsed Sextupole Magnet

A new injection system with a pulsed sextupole magnet (PSM) has been installed into the Photon Factory storage ring (PF-ring). In general, the pulsed local bump with several kicker magnets is employed for beam injection, in order to reduce coherent dipole oscillations in the injected beam. However, it is difficult to make a perfect closed bump using kicker magnets, due to field errors, timing jitters and non-linear magnetic field effects (similar to sextupole magnets) inside the bump. This is one of the problems to be overcome for successful top-up injection. To reduce oscillations of the stored beam caused by imperfections of the closed bump, we have proposed beam injection using PSM [1-2]. The injected beam is captured into the ring acceptance region by the PSM kick, the strength of which increases as the square of the distance from the magnetic field center. On the other hand, the stored beam passes through the center of the PSM, where the magnetic field is almost zero.

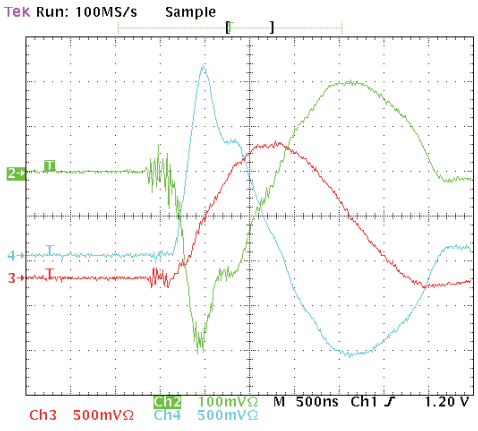

Figure 31
Typical waveforms measured at a charging voltage of 16.7 kV. The solid red line represents the excitation current (Ch3). The solid green and cyan lines represent the output signals of the short coil (Ch2) and the long coil (Ch4), respectively. The search coil is placed at a horizontal location of 15 mm from the magnetic pole center.

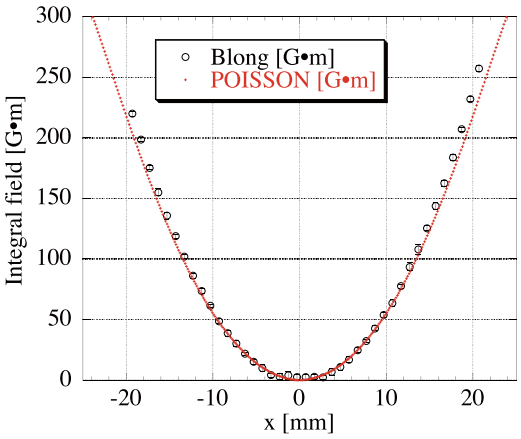

Figure 32
Horizontal distribution of the integrated magnetic field. Open circles (black) show the measured result using the long coil, and the dotted line (red) shows the calculated results from the POISSON code.

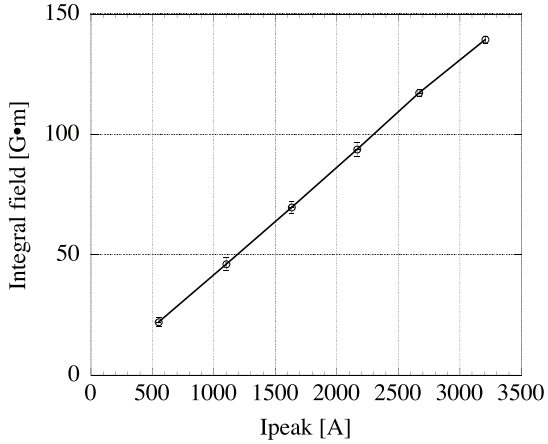

Figure 33
Excitation curve of the integrated magnetic field as a function of the peak current of the pulsed power supply.

Since the kick to the stored beam is quite weak, the perturbation during the injection becomes very small. Therefore, the new injection scheme is expected to be very suitable for top-up injection.

A PSM with a core length of 300 mm and a bore radius of 33 mm was produced [2]. The magnet was laminated from silicon steel sheets 0.15 mm thick, and the coil was made from one-turn copper with a diameter of 15 mm. The PSM is air-cooled without using a blower. The requirement for the integrated magnetic field of the PSM is 120 Gauss-m at a horizontal displacement of 15 mm from the magnet center, where the injection beam passes. This strength corresponds to a K_2 (= B"L/Bρ) of 13 m^{-2}, where B" is the field gradient, L is the core length and Bρ is the magnetic rigidity.

The pulsed power supply used for the system has an output current with a half-sine pulse shape with a full width of 2.4 μsec and a maximum charging voltage of 40 kV. The total inductance is estimated to be 4.3 μH. The charging voltage required for beam injection is estimated to be 16.7 kV at a peak current of 3000 A. Repetition frequencies of up to 25 Hz are available.

We measured the pulsed current using a current transformer (CT), and the pulsed magnetic field using

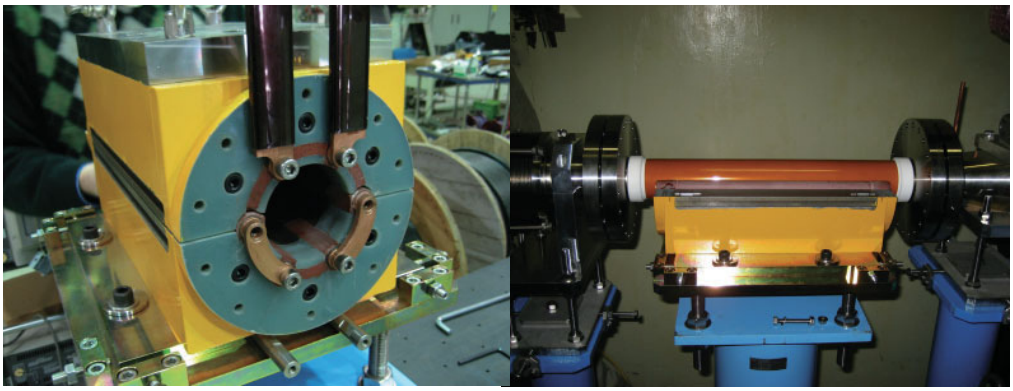

Figure 34
Photographs of the PSM: a front view of the magnet (yellow) is shown in the left photo, and the ceramic chamber (white) on the half-split magnet in the right photo. The chamber is protected by a 100 μm thick film (brown).

two search coils: a short 5 mm × 5 mm rectangular coil and a long 5 mm × 600 mm rectangular coil. The short search coil was employed for measuring the distribution of the magnetic field along the longitudinal direction and the long search coil was used to measure the integrated magnetic field. Each coil was made from single-turn fine copper wire attached to a glass epoxy bar. Figure 31 shows the typical waveforms measured at a charging voltage of 16.7 kV. The magnetic field was evaluated by integrating the output voltage of the search coil.

Figure 32 shows the horizontal distribution of the integrated field measured at a peak current of 3000 A. The result is compared with the integrated field calculated using the POISSON code [3]. The distribution shows a parabolic shape, and the magnetic field around the center of the PSM is nearly zero. The measured values for large horizontal displacements are slightly larger than the calculated values, since the effective length of the PSM is 320 mm. Figure 33 shows the excitation curve as a function of peak current for 500 to 3200 A at a horizontal displacement of 15 mm from the PSM center. The integrated field linearly increases from 20 to 140 Gauss-m without saturation.

The PSM was installed in the north 8.9 m long straight section in the PF-ring (Fig. 34). A ceramic chamber is employed to reduce eddy currents, which cause distortion and delay of the pulsed magnetic field. The thickness of the ceramic chamber is 3 mm, and the clearance between the chamber and the magnetic pole is 0.5 mm. The inner side is coated with a 3 μm layer of titanium.

The arrival time of the injected beam was monitored using a wall current monitor, and the excitation timing of the PSM was carefully adjusted so that the beam was efficiently captured into the ring. A single-bunch beam was used for the timing adjustments. Figure 35 shows the waveform recorded by the digital oscilloscope (Tektronics TSD748) the first time we successfully injected and stored a real beam using the PSM. Since the revolution period of the PF-ring is about 0.6 μsec, a half-sine pulse with a full width of 1.2 μsec or less is preferable for beam injection. However, the existing pulsed power supply has a full width of 2.4 μsec. It is inevitable that the injected beam receives a second kick from the PSM.

Next, we tried to accumulate the beam up to a current of 450 mA in multi-bunch mode. Figure 36 shows the trend of the stored beam current. Injection was firstly

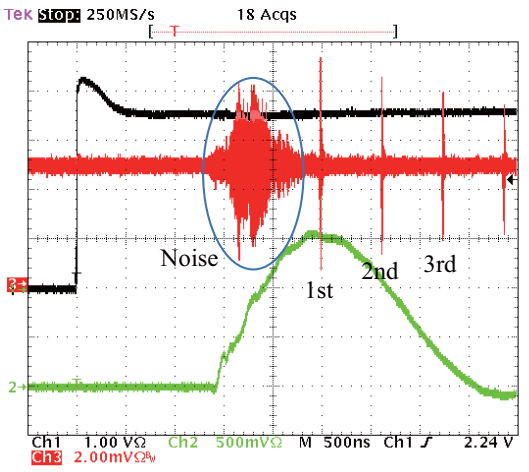

Figure 35
Typical waveform during the adjustment of the excitation timing of the PSM measured using a digital oscilloscope. The lines represent the discharge trigger (black), the signal from the current transformer of the pulsed power supply (green), and the wall current monitor of the ring (red). The interval of the red line shows the revolution time. The injection was made at the peak of the pulse. There still exists a very small magnetic field at the third turn.

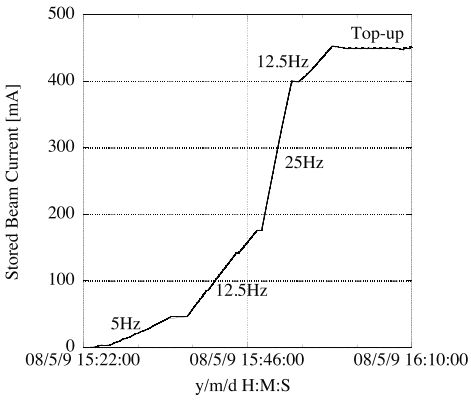

Figure 36
Stored beam current as a function of elapsed time. The beam was injected mainly using the PSM, but the usual injection system was also used at a repetition rate of 25 Hz in order to reduce experiment time.

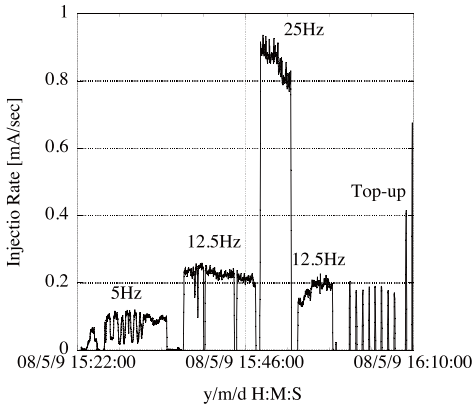

Figure 37
Injection rate as a function of elapsed time for the same conditions as Fig. 36.

carried out at a repetition frequency of 5 Hz, followed by an increase to 12.5 Hz. In order to save time and compare injection rates, the usual PF-ring injection system was then used until beam current exceeded 400 mA, when PSM injection was resumed. Figure 37 shows the injection rate as a function of elapsed time. Injection rates with high stored currents were lower than with low stored currents. The reason for this will be examined in detail in the next experiments. It was possible to inject up to a stored current of 450 mA, and maintain this current with continuous (top-up) injection using the PSM.

This is the first demonstration of PSM beam injection in an electron storage ring anywhere in the world. In the next experiment, we will examine the performance of the PSM beam injection in detail.

REFERENCES

[1] Y. Kobayashi and K. Harada, *Proc. of the EPAC* (2006) 3526.
[2] H. Takaki, N. Nakamura, Y. Kobayashi. K. Harada, T. Honda, T. Miyajima and S. Nagahashi, *Proc. of the PAC* (2007) 231.
[3] POISSON/SUPERFISH, *Los Alamos National Laboratory Report*, LA-UR-96-1834.

2-7 Renovation of the SR Monitor and Measurement of Emittanace

The SR monitor system at BL21 was renovated in order to measure the emittance of the electron beam at the Photon Factory after the straight sections upgrade project. The SR extraction system in the beam diagnostics beamline BL21 originally used a water-cooled copper mirror, which had become seriously damaged by SR irradiation over a long period of time. We replaced this mirror system with a new system which has a water-cooled beryllium mirror. A schematic drawing and photograph of the beryllium mirror are shown in Fig. 38.

A glass window sealed with a metal O-ring was used in the new system. The transparent wavefront error of the window is less than $\lambda/10$ [1]. Thermal deformation of the mirror due to strong irradiation by the X-ray components of the SR is one of the serious problems to be solved for the SR monitor. This deformation was measured by ray tracing based on the Hartmann method [2]. A schematic drawing of the setup used is shown in Fig. 39. A 10 $\times$ 10 square-array mask is positioned just after the mirror to sample the rays. The diameter of holes is 1 mm, and the separation between the holes is 5 mm.

SR is used as the light source for the ray tracing. The propagation of the rays is observed on a screen 8 m downstream of the square mask. The mirror was deformed from its initial shape due to SR irradiation. Since the current-dependent deformation was smaller than this initial deformation, we measured changes in mirror shape for ring currents higher than 300 mA, relative to the shape at 300 mA. The results are shown in Fig. 40. The figure indicates mirror shapes those observed from backside.

The mirror was deformed by 6μm with a ring current increase from 320mA to 450 mA. Near the right-side edge (corresponding to upside of the mirror) in Fig. 40 is deformed as defocus manner due to fixation of the mirror.

A focusing system is installed to observe a qualitative image of the electron beam. To reduce the effects of the thermal deformation of the beryllium mirror as mentioned above, the entrance pupil of the objective lens of the focusing system is defined by a square-aperture mask. A typical image of the beam is shown in Fig. 41.

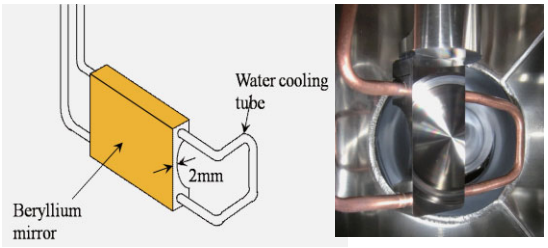

Figure 38
Schematic drawing and photograph of the water-cooled beryllium mirror.

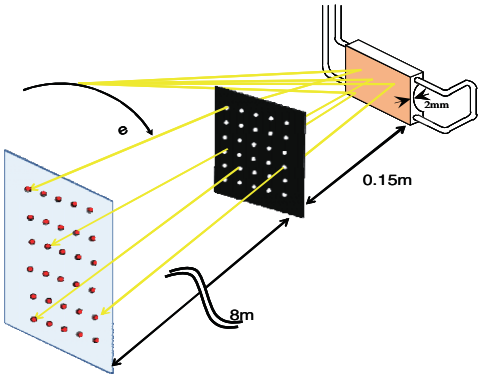

Figure 39
Schematic drawing of the setup used for the ray tracing measurement.

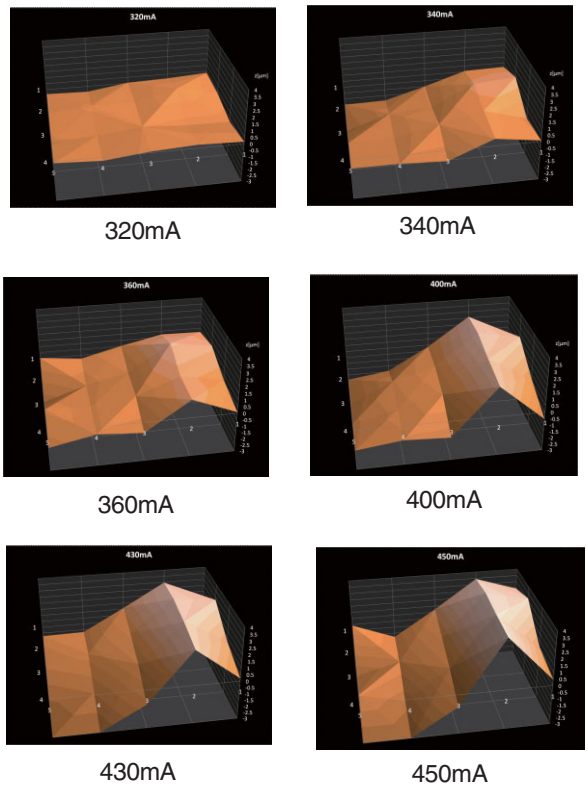

Figure 40
Changes in mirror shape compared to the shape at a current of 300 mA.

Figure 41
Qualitative image of the electron beam observed using the focusing system.

Quantitative measurements of electron beam size are performed by using the SR interferometer [2]. For measurements in the horizontal direction, a SR interferometer with retro-focus optics [3] was used to measure the large beam sizes. Since the actual separation of the double slit will change due to thermal deformation of the beryllium mirror, we must correct for this effect. The ideal separation of the double slit, with no deformation of the beryllium mirror, is evaluated from ray tracing using a single hole of the square-array mask [4] of the Hartmann ray-tracing system. Results of measurements of the intrinsic separation of the double slit in both the horizontal and vertical directions are shown in Fig. 42.

In these measurements, the actual separations of the double slits are 4 mm in the horizontal direction and 30 mm in the vertical direction. Since the magnification of the retro-focus optics in the horizontal SR interferometer is set to a value of 2, the actual separation of the double slit is about twice the ideal separation. The rather large difference between the actual and ideal separations in the vertical direction is due to permanent deformation of beryllium mirror. Current dependences of the ideal separations due to changes in mirror shape are also observed. By using the measured intrinsic separations of the double slit, we measured the current dependence of the beam sizes in the horizontal and vertical directions for currents from 50 mA to 400 mA. The results for the current dependence of the beam sizes before and after this correction are shown in Fig. 43. In the vertical direction the current dependence of the beam size is small. In the horizontal direction, the beam size is almost constant for currents from 50 mA to 270 mA, but a sudden jump, of around 20%, is observed around 270 mA.

To investigate this jump in beam size, we have measured the energy spread of the electron beam via a bunch length measurement using a streak camera. Since the dispersion function is not zero at the source point of BL21, information on the energy spread is also necessary in order to evaluate the emittance of the electron beam. The results of the measurements of longitudinal beam profile at currents below and above 270 mA are shown in Fig. 44.

The bunch length at currents lower than 270 mA is 33 ps. At currents above 270 mA, bunch lengths of 40 ps and 60 ps are observed. The relationship between bunch length and energy spread is given by the equation

$$\sigma_\tau = T_0 \sqrt{\frac{\alpha E_0}{2\pi h e V_{rf} \sin\phi_s}} \left(\frac{\Delta E}{E}\right).$$

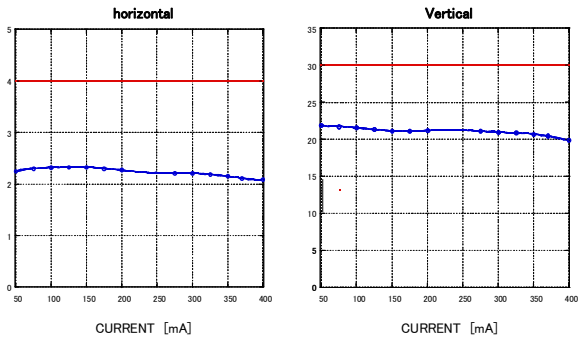

Figures 42
Intrinsic separation of the double slit in both horizontal and vertical directions.

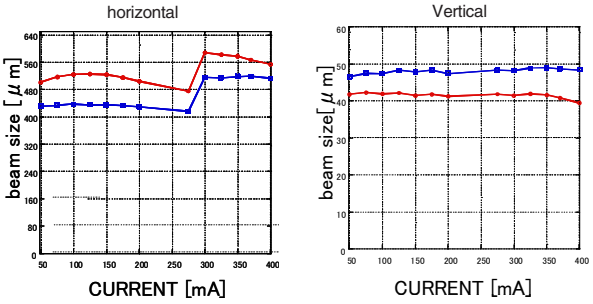

Figure 43
Current dependence of the beam sizes. The red lines denote the beam sizes evaluated using the actual separation of the double slit. The blue lines denote the beam size evaluated using the intrinsic separation of double slit.

Table 4 Results of the emittance and coupling measurements, along with the design values.

	σ_χ [μm]	σ_χ [μm]	ε_χ [nmrad]	ε_y [nmrad]	Coupling(%)
Measurement result	416±5	48±1	38.7±1.3	0.244±0.001	0.63±0.11
design values	413	59.4	35.5	0.355	1

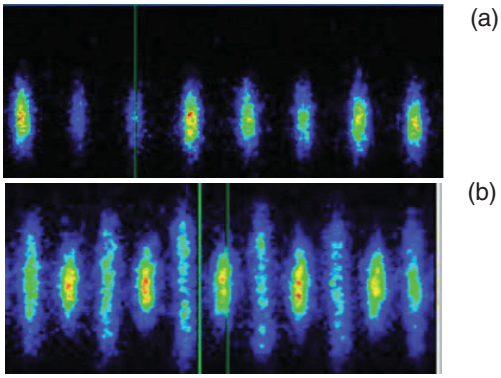

Figure 44
Longitudinal beam profile measured (a) below, and (b) above 270 mA.

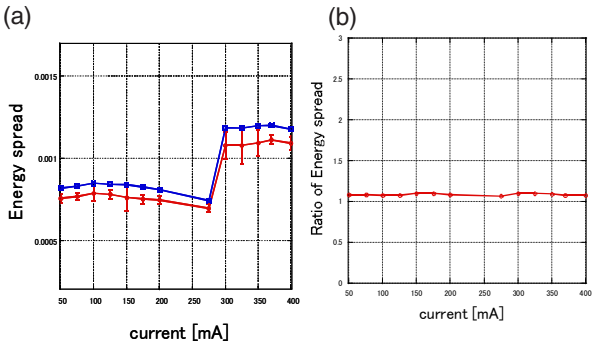

Figure 45
(a) The results of the energy spread measurements. The red line denotes energy spread evaluated from bunch length, and the blue line denotes energy spread evaluated from beam size. (b) Ratio between the energy spreads evaluated from beam size and from bunch length.

The energy spread evaluated using this equation is shown in Fig. 45 (a), along with the energy spread evaluated from the horizontal beam size measurements and the design emittance. The ratio of these is shown in Fig. 45 (b). The two results agree to within 10%.

Since the ratio of the two results is almost constant over the measured range of beam current, we can conclude that the increase in horizontal beam size above 270 mA is due to an increase in energy spread. The weak current dependence of the horizontal beam size, as shown in Fig. 43, can also be explained by comparison with the current dependence of the energy spread. From this evidence, we can conclude that the emittance of the electron beam has almost no current dependence. The emittance and coupling measurements are summarized in Table 4, along with the design values. The measured emittance agrees with the design value to within 10%. Taking into account that the precision of the measurements of the β and η functions are about 10%, we can conclude that the measured emittance of the PF ring is in good agreement with the design value.

REFERENCES

[1] T. Mitsuhashi and K. Kanazawa, *Proc. 13th Sym. on Accel. Sci. and Tec.* (2001) 387.
[2] T. Mitsuhashi , *Proceedings of BIW04* (2004).
[3] J.W. Flanagan H. Hukuma, S. Hiramatsu and T. Mitsuhashi, *PAC05*, (2005) 3150 .
[4] T. Mitsuhashi and M. Tadano, *Proc. APAC01* (2001) 704.